

Global structure of regular tori in a generic 4D symplectic map

S. Lange,^{1,2} M. Richter,^{1,2} F. Onken,¹ A. Bäcker,^{1,2} and R. Ketzmerick^{1,2}

¹⁾ *Technische Universität Dresden, Institut für Theoretische Physik and Center for Dynamics, 01062 Dresden, Germany*

²⁾ *Max-Planck-Institut für Physik komplexer Systeme, Nöthnitzer Straße 38, 01187 Dresden, Germany*

(Dated: 10 November 2018)

For the case of generic 4D symplectic maps with a mixed phase space we investigate the global organization of regular tori. For this we compute elliptic 1-tori of two coupled standard maps and display them in a 3D phase-space slice. This visualizes how all regular 2-tori are organized around a skeleton of elliptic 1-tori in the 4D phase space. The 1-tori occur in two types of one-parameter families: (α) Lyapunov families emanating from elliptic-elliptic periodic orbits, which are observed to exist even far away from them and beyond major resonance gaps, and (β) families originating from rank-1 resonances. At resonance gaps of both types of families either (i) periodic orbits exist, similar to the Poincaré-Birkhoff theorem for 2D maps, or (ii) the family may form large bends. In combination these results allow for describing the hierarchical structure of regular tori in the 4D phase space analogously to the islands-around-islands hierarchy in 2D maps.

PACS numbers: 05.45.Jn, 05.45.-a, 45.20.Jj

For Hamiltonian systems with two degrees of freedom or two-dimensional area-preserving maps a detailed understanding of dynamics is well-established: Around stable periodic orbits one typically has invariant regular tori if their frequency is sufficiently irrational as predicted by the Kolmogorov-Arnold-Moser (KAM) theorem. For rational frequencies, the Poincaré-Birkhoff theorem predicts a chain of elliptic and hyperbolic periodic orbits. These structures can be directly visualized by two-dimensional plots of the dynamics providing a high level of intuition. In this paper we make progress towards a similar level of understanding for higher-dimensional systems using 3D phase-space slices to visualize the dynamics. For a 4D map we show that all regular 2-tori are organized around a skeleton of elliptic 1-tori, see Fig. 1. These are associated either with elliptic-elliptic periodic orbits or with rank-1 resonances. The visualization allows for an intuitive understanding of the organization of regular tori and their hierarchy in higher-dimensional systems analogously to 2D maps.

dimensional symplectic maps, which, e.g., arise from autonomous Hamiltonian systems with $f+1$ degrees of freedom or time-periodically driven systems with f degrees of freedom.

For 2D symplectic maps the organization of structures in phase space is well understood¹: Around elliptic fixed points and periodic orbits one has 1D regular tori with sufficiently irrational frequencies as predicted

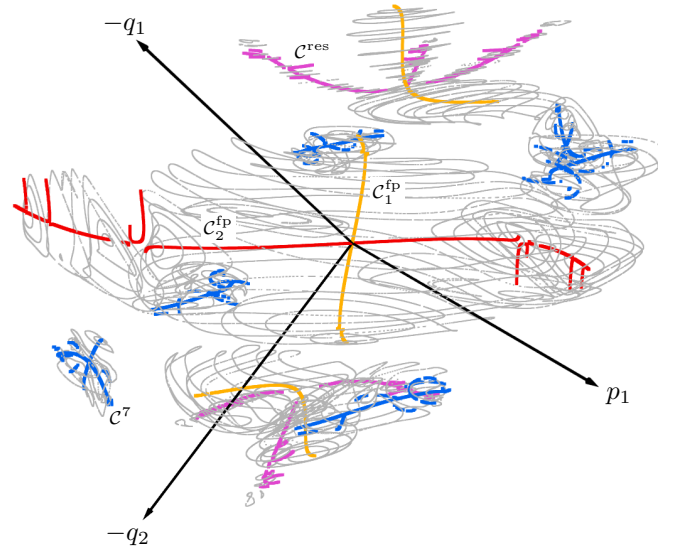


FIG. 1. Central lines C_1^{fp} , C_2^{fp} , C_7 , C^{res} (orange, red, blue, magenta) in the 3D phase-space slice representing families of 1-tori of type (α) $\mathcal{M}_1^{\text{fp}}$, $\mathcal{M}_2^{\text{fp}}$, \mathcal{M}_7 and type (β) \mathcal{M}^{res} for two coupled standard maps, Eq. (1). Around the central lines the 2-tori (gray) are organized. From the elliptic-elliptic fixed point \vec{u}_{fp} the two central lines C_1^{fp} , C_2^{fp} (orange, red) emanate, and continue beyond the large gaps. The central lines C^{res} (magenta) arise from a $-1 : 3 : 0$ resonance. For a rotating view see⁷⁴

I. INTRODUCTION

The dynamics of higher-dimensional Hamiltonian systems is intensively studied in many areas of physics, chemistry, and mathematics¹, such as the solar system²⁻⁴, particle accelerators⁵, atoms and molecules⁶⁻¹¹, as well as KAM-theory¹²⁻¹⁵. Especially important phenomena are Arnold diffusion^{1,4,16,17}, which exclusively occurs in higher-dimensional systems, and power-law trapping or stickiness of chaotic orbits¹⁸⁻²², whose mechanism is still unknown for these systems. To investigate these questions it is particularly convenient to study 2f-

by the Kolmogorov-Arnold-Moser (KAM) theorem. This surrounding of an elliptic point is referred to as a regular island. In contrast, resonant regular tori break up in the non-integrable case into chains of elliptic and hyperbolic periodic orbits according to the Poincaré-Birkhoff theorem. This gives rise to a whole hierarchy of regular islands, e.g., islands-around-islands²³. This hierarchy along with its affiliated structures, like stable and unstable manifolds, governs the dynamics in phase space.

For higher-dimensional maps the organization of regular tori in phase space is more complicated: For a $2f$ -dimensional symplectic map the corresponding phase space in general contains regular tori of dimensions $d = 0, \dots, f$ ^{12-14,24}, in the following denoted as d -tori. The behavior normal to lower-dimensional tori ($0 < d < f$) and fixed points ($d = 0$) can be an arbitrary combination of hyperbolic and elliptic components²⁵⁻²⁷. A d -torus is called elliptic or hyperbolic if all its normal components are elliptic or hyperbolic²⁵. Hyperbolic tori, also called whiskered tori, are important for many dynamical properties of a system, including Arnold diffusion^{11-13,16,28}. The regular tori have a hierarchical ordering in the sense that Cantor families of elliptic d -tori are arranged around elliptic $(d - 1)$ -tori for $0 < d \leq f$ in an intricate way^{25,26,29}. In particular, the elliptic (lower-dimensional) tori are investigated in the context of KAM-theory^{15,28-31}, important for the description of (Hopf)-bifurcations^{27,32-34}, and one origin of stickiness^{19,35-37}. Furthermore, the hierarchical ordering of elliptic tori has been studied for the hydrogen atom in crossed fields^{8,38} and in the context of Hamilton-Hopf bifurcations^{27,39}, and observed in solar systems^{40,41}. However, despite the available analytical and numerical results a complete description of the phase-space structures and their geometry is still missing for higher-dimensional systems. Most of the mentioned results have been obtained by normal form tools^{12-15,24,26,30} or other perturbative schemes^{33,34,39} and therefore only cover near-integrable systems or the vicinity of invariant objects, e.g., fixed points. However, many practical applications are concerned with non-perturbative systems^{8,10,31,38}. Thus, it is particularly relevant to investigate the phase-space structures in systems far from integrability and far from fixed points.

The aim of this paper is to investigate and visualize the organization of regular tori of generic 4D symplectic maps to gain an understanding similar to the insights already available for 2D maps. For this we use a new numerical algorithm to compute elliptic 1-tori from their surrounding 2-tori. We employ the 3D phase-space slices⁴² to simultaneously display both 1- and 2-tori, see Fig. 1. The 3D impression is considerably enhanced when one rotates the figure with standard 3D graphics. For the convenience of the reader for all 3D phase-space slices in this paper videos with rotating camera position are given in the supplemental material⁷⁴. The 3D phase-space slices clearly visualize that families of elliptic 1-tori form a skeleton for the surrounding 2-tori. We show that two types of such

families can be distinguished depending on whether they are associated with (α) an elliptic-elliptic fixed point (or elliptic-elliptic periodic orbit) or (β) a rank-1 resonance. The former families originate from the center submanifolds of the elliptic-elliptic fixed points and are also called *Lyapunov families of invariant curves*^{15,27}, while the latter are fundamentally different. We explain the origin of this type of families in detail based on results concerning the break-up of resonant 2-tori³⁰ and frequency analysis⁴³. Furthermore, we find two kinds of resonance gaps which interrupt the skeleton of elliptic 1-tori: (i) Periodic orbits exist at rational intrinsic frequencies, similar to the Poincaré-Birkhoff theorem for 2D maps, or (ii) large bends of the skeleton may occur at resonances involving the normal component. In combination of these results we generalize the islands-around-islands hierarchy known from 2D maps to the regular tori in the 4D phase space, based on the hierarchy of families of 1-tori.

This paper is organized as follows: In Sec. II A we introduce the map and review the 3D phase-space slices. In Sec. II B they are used to visualize the 1- and 2-tori and are related to 3D projections. Sec. II C presents a frequency analysis of the 1- and 2-tori. In Sec. II D the origin of the second type of families of 1-tori is explained and in Sec. II E the resonance gaps are discussed. In Sec. III the hierarchical structure of the 4D phase space is described. Finally, Sec. IV gives a summary and an outlook. The algorithm to compute 1-tori is presented in Appendix A and a review and illustration of the break-up of resonant 2-tori is given in Appendix B.

II. ORGANIZATION OF PHASE SPACE BY 1-TORI

A. Coupled standard maps and 2-tori

As a concrete example to study the organization of phase space in 4D maps we consider the prototypical system of two coupled standard maps⁴⁴

$$\begin{aligned} p'_1 &= p_1 + \frac{K_1}{2\pi} \sin(2\pi q'_1) + \frac{\xi_{12}}{2\pi} \sin(2\pi(q'_1 + q'_2)) \\ p'_2 &= p_2 + \frac{K_2}{2\pi} \sin(2\pi q'_2) + \frac{\xi_{12}}{2\pi} \sin(2\pi(q'_1 + q'_2)) \\ q'_1 &= q_1 + p_1 \\ q'_2 &= q_2 + p_2 \end{aligned} \quad (1)$$

where $p_1, p_2, q_1, q_2 \in [-1/2, 1/2)$ and periodic boundary conditions are imposed in each coordinate. The resulting map is symplectic. The parameters K_1 and K_2 control the nonlinearity of the individual 2D standard maps in (p_1, q_1) and (p_2, q_2) , respectively. The parameter ξ_{12} introduces a coupling between the two degrees of freedom. We choose $K_1 = -2.25$, $K_2 = -3.0$ and $\xi_{12} = 1.0$, such that the system is strongly coupled and far from integrability⁴². The origin $\vec{u}_{\text{fp}} = (p_1, p_2, q_1, q_2) = (0, 0, 0, 0)$ is an elliptic-elliptic fixed point. The eigenvalues $(\lambda_1^{\text{fp}}, \bar{\lambda}_1^{\text{fp}}, \lambda_2^{\text{fp}}, \bar{\lambda}_2^{\text{fp}})$ of the linearized

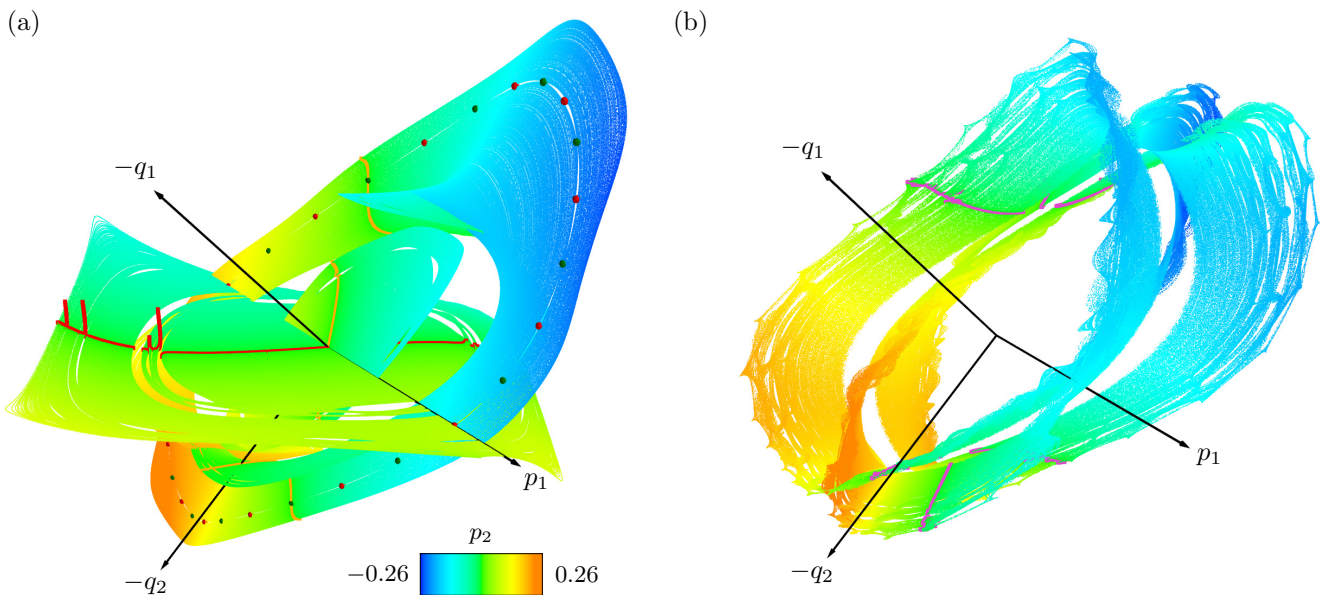


FIG. 2. Visualization of the 2D Cantor manifolds formed by the families of 1-tori $\mathcal{M}_1^{\text{fp}}$, $\mathcal{M}_2^{\text{fp}}$, \mathcal{M}^{res} . For a selection of 1000 1-tori (excluding the strong bends of $\mathcal{M}_2^{\text{fp}}$) 2000 iterates under the map (1) are computed and then projected on (p_1, q_1, q_2) . The value of p_2 is encoded in color. The central lines $\mathcal{C}_1^{\text{fp}}$, $\mathcal{C}_2^{\text{fp}}$, \mathcal{C}^{res} , which are the intersections of the families of 1-tori with $p_2 = 0$, are shown in the same colors as in Fig. 1. (a) Families $\mathcal{M}_1^{\text{fp}}$ and $\mathcal{M}_2^{\text{fp}}$. The spheres in a gap of $\mathcal{M}_1^{\text{fp}}$ correspond to two elliptic-elliptic (red) and two hyperbolic-elliptic (green) periodic orbits of period 7. (b) Family \mathcal{M}^{res} corresponding to the $-1 : 3 : 0$ resonance. For a rotating view see⁷⁴

dynamics around \vec{u}_{fp} are $(\exp(\pm i 2\pi\nu_1^{\text{fp}}), \exp(\pm i 2\pi\nu_2^{\text{fp}}))$ with $(\nu_1^{\text{fp}}, \nu_2^{\text{fp}}) = (0.30632, 0.12173)$ and corresponding eigenvectors $(\vec{v}_{1a}^{\text{fp}}, \vec{v}_{1b}^{\text{fp}}), (\vec{v}_{2a}^{\text{fp}}, \vec{v}_{2b}^{\text{fp}})$.

An orbit started at some initial point in the 4D phase space leads to a sequence of points (p_1, p_2, q_1, q_2) under the map (1). Such an orbit can be visualized by using a 3D phase-space slice Γ_ε , defined by thickening a 3D hyperplane Γ in the 4D phase space⁴². Explicitly, we consider the slice defined by

$$\Gamma_\varepsilon = \left\{ (p_1, p_2, q_1, q_2) \mid |p_2 - p_2^*| \leq \varepsilon \right\}. \quad (2)$$

with $p_2^* = 0$ and $\varepsilon = 10^{-4}$ as it provides a good view of most structures of the map (1). Whenever a point of an orbit lies within Γ_ε , the remaining coordinates (p_1, q_1, q_2) are displayed in a 3D plot. Objects of the 4D phase space will typically appear in the 3D phase-space slice with a dimension reduced by one, provided the object intersects with the slice. Thus, a typical 2-torus will lead to two or more 1D lines. A periodic orbit will in general not be visible, unless at least one of its points lies in the 3D phase-space slice.

In Fig. 1 several initial conditions leading to regular orbits are selected and iterated until for each of them 4000 points are contained in the 3D phase-space slice. They lead to 1D rings shown in gray in Fig. 1. In the center of phase space one has the elliptic-elliptic fixed point \vec{u}_{fp} , which is surrounded by a two-parameter family

of 2-tori. Further away the 2-tori form different clusters, each approximately filling a 4D volume in the 4D phase space. This regular region is embedded in a chaotic sea (not shown) formed by chaotic orbits. These structures have previously been discussed in detail⁴².

B. Skeleton of 1-tori

Fig. 1 shows that the 2-tori seem to be organized in some way even far away from the elliptic-elliptic fixed point \vec{u}_{fp} . We demonstrate in this section that the 2-tori are grouped around families of elliptic 1-tori. Note that in the following 1-torus always refers to elliptic 1-torus.

In order to understand this organization in phase space, we start by considering a 2-torus and contract its minor radius to zero using the algorithm described in Appendix A. The resulting object is a 1-torus. If such a 1-torus intersects with the 3D phase-space slice it will typically lead to two or more points in the slice. Performing this contraction procedure for many 2-tori one gets the result shown in Fig. 1: The points of the 1-tori approximately form lines in the 3D phase-space slice. This means that the 1-tori form one-parameter families \mathcal{M} in the 4D phase space. We denote their representation in the 3D phase-space slice as *central lines* \mathcal{C} . In Fig. 1 all 2-tori appear to be centered around one of these lines. This is particularly well visible, e.g., for the tori around

the center lines $\mathcal{C}_1^{\text{fp}}$ (orange) and \mathcal{C}^{res} (magenta). Thus, the families of 1-tori \mathcal{M} provide the skeleton for the surrounding 2-tori. The 1-tori composing a particular family \mathcal{M} can also be displayed by 3D projections encoding the value of the projected coordinate by a color scale^{45,46}, see Fig. 2.

We now discuss the two types of families of 1-tori \mathcal{M} . This will be done starting from their representation as central lines \mathcal{C} in the 3D phase-space slice, see Fig. 1:

(α) The central lines $\mathcal{C}_1^{\text{fp}}$ and $\mathcal{C}_2^{\text{fp}}$ shown in orange and red in Fig. 1 both emanate from the central elliptic-elliptic fixed point \vec{u}_{fp} . Further away from \vec{u}_{fp} one has visible gaps but the central lines continue beyond them. Such gaps result from resonances, see Secs. II C and II E, and occur on arbitrarily fine scales along the central lines. Thus more precisely, they are *Cantor central lines*. In the 3D projection in Fig. 2 (a) the families of 1-tori $\mathcal{M}_1^{\text{fp}}$ and $\mathcal{M}_2^{\text{fp}}$ compose two 2D Cantor manifolds. These manifolds $\mathcal{M}_1^{\text{fp}}$ and $\mathcal{M}_2^{\text{fp}}$ only intersect in the central elliptic-elliptic fixed point \vec{u}_{fp} ⁴⁷. At \vec{u}_{fp} the two 2D planes spanned by the eigenvectors $(v_{1a}^{\text{fp}}, v_{1b}^{\text{fp}})$ and $(v_{2a}^{\text{fp}}, v_{2b}^{\text{fp}})$ of the linearized map are tangential to the manifolds $\mathcal{M}_1^{\text{fp}}$ and $\mathcal{M}_2^{\text{fp}}$. Also the frequencies of the 1-tori converge to those of \vec{u}_{fp} , see Sec. II C.

These features remind of the invariant manifolds predicted by the Lyapunov center theorem⁴⁸. However, since the system is not integrable, $\mathcal{M}_1^{\text{fp}}$ and $\mathcal{M}_2^{\text{fp}}$ are Cantor manifolds, interrupted by many gaps due to resonances. They are called *Lyapunov families of invariant curves*^{15,27} or *Cantorian central submanifolds*²⁶ and have previously been studied in the near-integrable regime^{39,49,50}. Hence, the central lines $\mathcal{C}_1^{\text{fp}}$ and $\mathcal{C}_2^{\text{fp}}$ represent the Lyapunov families $\mathcal{M}_1^{\text{fp}}$ and $\mathcal{M}_2^{\text{fp}}$ of \vec{u}_{fp} , respectively. We observe that these families also exist far away from the elliptic-elliptic fixed point \vec{u}_{fp} and continue beyond large resonance gaps.

The central lines \mathcal{C}^7 shown in blue in Fig. 1 are associated with two elliptic-elliptic periodic orbits of period 7. Each torus consists of seven disjoint parts in the 4D phase space⁴². The central lines emanating from each point of the elliptic-elliptic period-7 orbits are conceptually the same as the central lines of the central elliptic-elliptic fixed point \vec{u}_{fp} . In Appendix B it is explained that the period-7 orbits exist due to a rank-2 resonance.

(β) The central lines \mathcal{C}^{res} shown in magenta in Fig. 1 are fundamentally different from $\mathcal{C}_1^{\text{fp}}$, $\mathcal{C}_2^{\text{fp}}$, and \mathcal{C}^7 . They occur as two groups of three branches, each group emerging near the central line $\mathcal{C}_1^{\text{fp}}$ (orange). Most importantly, there is no fixed point or periodic orbit from which the central lines \mathcal{C}^{res} originate. The visualization of the family of 1-tori \mathcal{M}^{res} in Fig. 2 (b) has a very different topology from case (α) in Fig. 2 (a). It is shown in Sec. II D, that such types of families of 1-tori result from broken resonant 2-tori of a rank-1 resonance. In the case of \mathcal{C}^{res} it is the $-1 : 3 : 0$ resonance. Still, we make the same observations regarding resonance gaps as in case (α), see Sec. II E.

Note that there is a case where the types (α) and (β) coincide. Such families of 1-tori are discussed in Sec. III.

C. 1-tori in the frequency plane

In order to understand the influence of resonances we now relate the observations in phase space to a frequency analysis^{43,51} which associates with each 2-torus its two fundamental frequencies $(\nu_1, \nu_2) \in [0, 1]^2$. These are displayed in the frequency plane, see Fig. 3, where the gray points represent 2-tori obtained by starting 10^8 initial conditions with randomly chosen $p_1, p_2, q_1, q_2 \in [-0.2, 0.2]$ in the 4D phase space. Each frequency pair is calculated from $N = 4096$ iterations. To decide whether an orbit is regular we use the frequency criterion

$$\max(|\nu_1 - \tilde{\nu}_1|, |\nu_2 - \tilde{\nu}_2|) < 10^{-7}, \quad (3)$$

where the frequency pair $(\tilde{\nu}_1, \tilde{\nu}_2)$ is calculated from N further iterations. This leads to nearly $3 \cdot 10^6$ regular 2-tori. Since the frequencies (ν_1, ν_2) are only defined up to a unimodular transformation^{38,52,53} we use the 3D phase-space slices to choose frequencies consistently⁴². The frequency plane is covered by resonance lines $m_1 : m_2 : n$, on which the frequencies fulfill

$$m_1 \cdot \nu_1 + m_2 \cdot \nu_2 = n \quad (4)$$

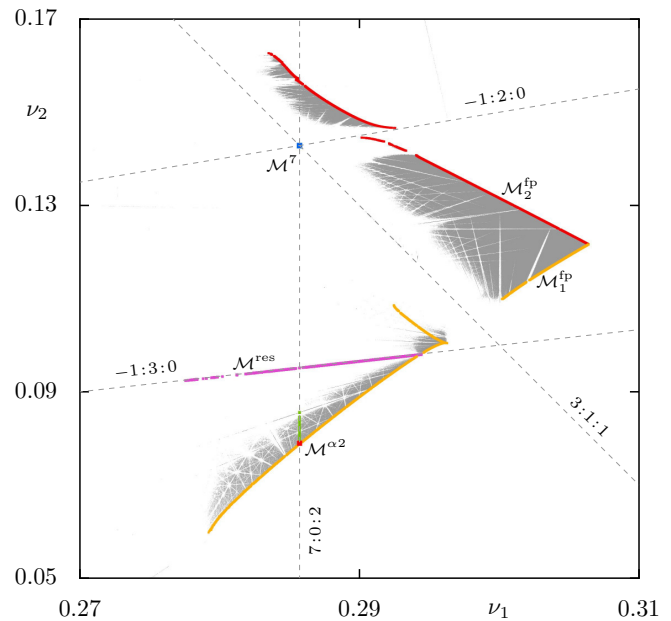


FIG. 3. Frequencies (ν_1, ν_2) of all 2-tori (grey). The largest gaps stem from the $3 : 1 : 1$ and $-1 : 2 : 0$ resonances. The frequencies of the fixed point \vec{u}_{fp} are $(\nu_1^{\text{fp}}, \nu_2^{\text{fp}}) = (0.30632, 0.12173)$. From there the (α) families of 1-tori $\mathcal{M}_1^{\text{fp}}$, $\mathcal{M}_2^{\text{fp}}$ (orange, red) emanate, forming the skeleton of the regular region. The frequencies for 1-tori of the (β) family \mathcal{M}^{res} (magenta) are all on the $-1 : 3 : 0$ resonance line and for the (α) families \mathcal{M}^7 (blue) on the point $(2/7, 1/7)$. The families $\mathcal{M}^{\alpha 2}$ (green) are discussed in Sec. III.

where m_1, m_2, n are integers with at least one being nonzero. The most important resonance lines are displayed in Fig. 3.

The two-parameter families of 2-tori in the 3D phase space slice directly correspond to areas in the frequency plane⁴². For example, the frequencies $(\nu_1^{\text{fp}}, \nu_2^{\text{fp}})$ of the elliptic-elliptic fixed point \vec{u}_{fp} correspond to the right-most tip. Large gaps due to resonances, like the $3 : 1 : 1$ and the $-1 : 2 : 0$, correspond to gaps in the 3D phase space slice, see Fig. 1.

In contrast to a 2-torus, the dynamics on a 1-torus is described by only one frequency, which is also called intrinsic frequency. For example, the frequency on $\mathcal{M}_1^{\text{fp}}$ (orange) corresponds to ν_1 and on $\mathcal{M}_2^{\text{fp}}$ (red) to ν_2 in Fig. 3. The frequency describing the normal behavior can be obtained from the limiting 2-tori or from the linearized dynamics normal to the 1-torus^{27,54}. This frequency is called normal or librating frequency. The families of 1-tori are indicated in Fig. 3 with colors corresponding to their central lines in Fig. 1. This allows to make the connection with the two types (α) and (β) of families of 1-tori \mathcal{M} represented by the central lines \mathcal{C} :

(α) The sharp edges emanating from the elliptic-elliptic fixed point \vec{u}_{fp} at $(\nu_1^{\text{fp}}, \nu_2^{\text{fp}})$ correspond to the families $\mathcal{M}_1^{\text{fp}}$ and $\mathcal{M}_2^{\text{fp}}$ (orange, red). The frequencies of the 2-tori emanate from these edges. In this sense, the 1-tori also organize the frequencies of the 2-tori. Moreover, one recognizes in the frequency plane that the gaps in the families \mathcal{M} and their central lines \mathcal{C} in Figs. 1 and 2 are due to resonances. Fig. 3 also nicely illustrates that the edges corresponding to $\mathcal{M}_1^{\text{fp}}$ and $\mathcal{M}_2^{\text{fp}}$ continue beyond large resonance gaps. Note that the frequencies of the 1-tori of \mathcal{M}^7 and their elliptic surrounding collapse to the point $(\nu_1, \nu_2) = (2/7, 1/7)$.

(β) The frequencies of the family of 1-tori \mathcal{M}^{res} (magenta) lie on the $-1 : 3 : 0$ resonance line in Fig. 3. The frequencies of their surrounding 2-tori also lie on this resonance line.

The reason that the families \mathcal{M}^7 and \mathcal{M}^{res} and their surrounding 2-tori collapse on a point or a line, respectively, in Fig. 3 is that here the frequencies are calculated with respect to the central elliptic-elliptic fixed point \vec{u}_{fp} . In Sec. III an adapted frequency analysis is performed for these cases.

D. Families of 1-tori from rank-1 resonances

We now discuss that families of 1-tori of type (β), such as \mathcal{M}^{res} , which do not correspond to Lyapunov families of elliptic-elliptic fixed points or periodic orbits, originate from broken 2-tori that fulfilled a rank-1 resonance condition. This follows by applying results of Todesco³⁰, which are obtained for the vicinity of an elliptic-elliptic fixed point, to arbitrary families of resonant 2-tori far away from a fixed point or even in the absence of a fixed point. This is reviewed and illustrated in Appendix B:

One of the results is that a 2-torus fulfilling a rank-1 resonance in an integrable 4D symplectic map breaks up into several 1-tori when a perturbation is added. More precisely, an equal number of elliptic and hyperbolic 1-tori remains after the break-up of the 2-torus. Since for each rank-1 resonance there is usually a one-parameter family of 2-tori in the integrable system we infer that in the perturbed system for each of these resonances a one-parameter Cantor family of elliptic 1-tori exists. The appearance of these families in phase space is governed by the position and dynamics of the original resonant 2-tori, see Appendix B.

The 1-tori of the central lines \mathcal{C}^{res} (magenta) in Fig. 1 originate from the one-parameter family of broken 2-tori whose frequencies lie on the $-1 : 3 : 0$ resonance line. This is in accordance with the frequencies of the 1-tori of the family \mathcal{M}^{res} in Fig. 3. Note that we only show the elliptic and not the hyperbolic 1-tori of the broken 2-tori in Figs. 1 and 2 (b). While \mathcal{M}^{res} is an example for a coupled rank-1 resonance, we make analogous observations for uncoupled rank-1 resonances, e.g., for the $7 : 0 : 2$ resonance in Appendix B.

E. Resonance gaps in the skeleton of 1-tori

As mentioned in the previous sections the skeleton of 1-tori is interrupted by gaps due to resonances. Two different types of such gaps are observed depending on whether the normal frequency is involved in the resonance:

(i) If the intrinsic frequency along a family of 1-tori crosses a rational number, we observe a chain of alternating elliptic-elliptic and elliptic-hyperbolic periodic orbits arranged on a 1D line. This reminds of a break-up of a resonant 1-torus according to the Poincaré-Birkhoff theorem in 2D maps. As an example, we show in Fig. 2 (a) two elliptic-elliptic and two elliptic-hyperbolic periodic orbits of period 7, forming a chain in the gap of the family $\mathcal{M}_1^{\text{fp}}$. As seen in Fig. 3, these period-7 orbits arise from the intersection (red) of the $7 : 0 : 2$ resonance (green) with the family $\mathcal{M}_1^{\text{fp}}$ (orange). The emanating families of 1-tori $\mathcal{M}^{\alpha 2}$ and their surrounding are discussed in Sec. III and shown in Fig. 4 (c).

(ii) If the frequencies along a family of 1-tori cross a resonance involving the normal frequency, the central lines in the vicinity of the resonance may bend on either side of the resonance gap. This is well visible in Fig. 1 for the big gap of the central line $\mathcal{C}_1^{\text{fp}}$ (orange) caused by the $3 : 1 : 1$ resonance and the gap of the central line $\mathcal{C}_2^{\text{fp}}$ (red) caused by the $-1 : 2 : 0$ resonance. This behavior coincides with a bending of the corresponding edges in the frequency plane, see Fig. 3. For a system which is far from being integrable this bending in phase space and the frequency plane can occur on large scales and can have substantial impact on the dynamics. For instance, the regular region around the larger bend of $\mathcal{C}_1^{\text{fp}}$ at the $3 : 1 : 1$ resonance is

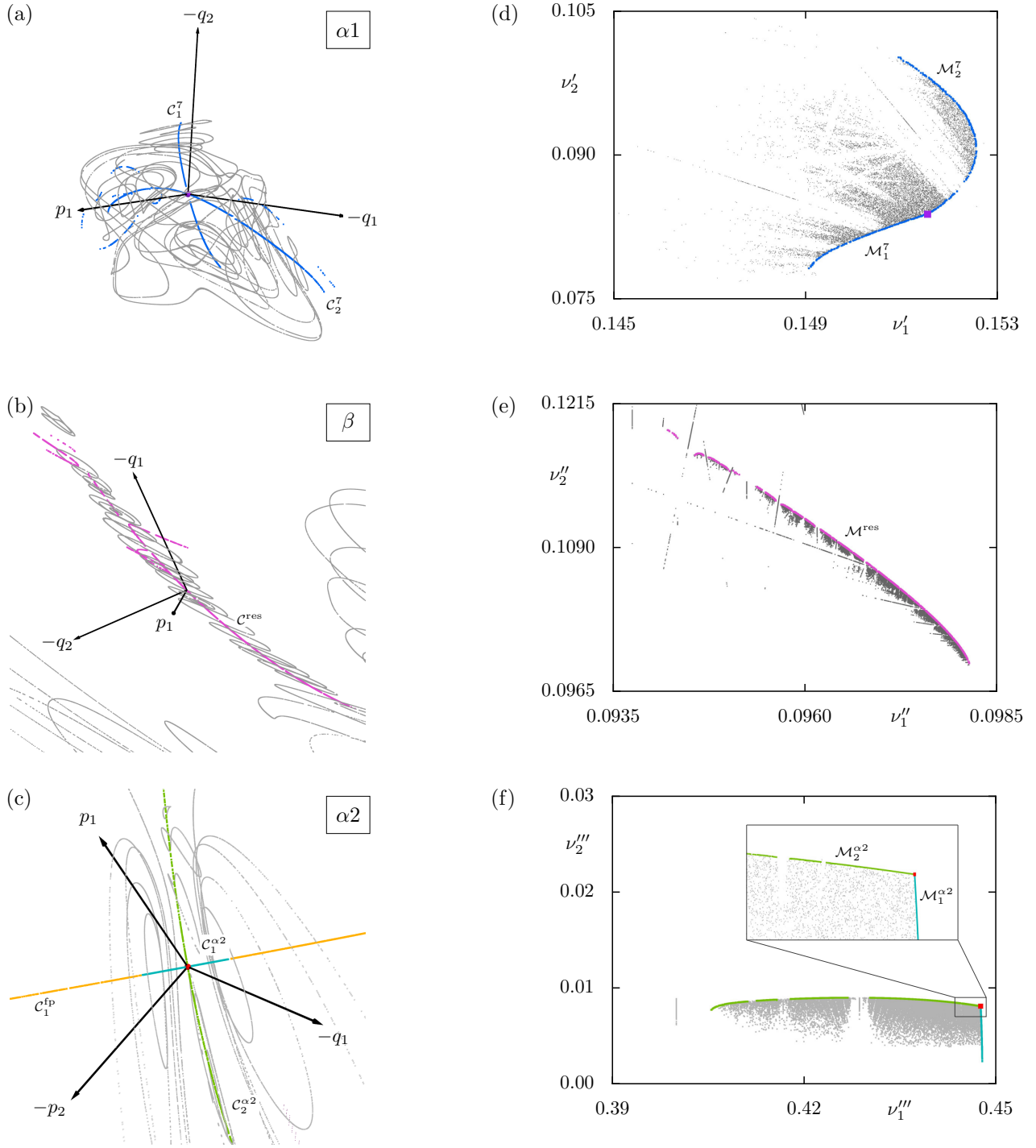


FIG. 4. First level of the hierarchy for (a) type ($\alpha 1$), (b) type (β), and (c) type ($\alpha 2$): Magnified views of Fig. 1 for (a) \mathcal{C}^7 around one point $\vec{u}_p = (0.0, 0.0, 0.083438087, 0.118666288)$ of the elliptic-elliptic period-7 orbit, (b) a branch of \mathcal{C}^{res} of the $-1 : 3 : 0$ resonance, and (c) central lines $\mathcal{C}_1^{\alpha 2}$ (turquoise) and $\mathcal{C}_2^{\alpha 2}$ (green) representing families of 1-tori $\mathcal{M}_1^{\alpha 2}$ and $\mathcal{M}_2^{\alpha 2}$ around one point $\vec{u}_{\alpha 2} = (0.115287658, -0.141621338, 0.0, 0.0)$ of the elliptic-elliptic period-7 chain. The slice condition is for (a), (b) $p_2^* = 0$ and $\varepsilon = 10^{-5}$ and for (c) $q_2^* = 0$ and $\varepsilon = 10^{-6}$. The coordinate system in (a) and (c) is moved to \vec{u}_p and $\vec{u}_{\alpha 2}$ respectively, and in (b) to an arbitrary point along \mathcal{C}^{res} . In (d), (e), and (f) the adapted frequencies are shown. In (a) and (d) the periodic point \vec{u}_p with frequencies $(\nu_1', \nu_2') = (0.1515, 0.0838)$ is marked by a magenta point. The two emanating families of 1-tori are colored the same for simplicity and have edges intersecting in the frequency plane with an angle close to π . In (c) and (f) the periodic point $\vec{u}_{\alpha 2}$ with frequencies $(\nu_1''', \nu_2''') = (0.4475, 0.0081)$ is marked by a red point. The inset in (f) shows a magnification around $\vec{u}_{\alpha 2}$. For a rotating view see⁷⁴

the main region for power-law trapping in the system²².

Note that for the $-1 : 3 : 0$ resonance the corresponding central line \mathcal{C}^{res} does not connect with the central line $\mathcal{C}_1^{\text{fp}}$ in Fig. 1. This is similar to the period tripling bifurcation for area-preserving 2D maps.

These observations correspond well to results about bifurcations of a 1-torus in volume-preserving 3D diffeomorphisms⁵⁵ and in a quasi-periodically forced Hamiltonian oscillator⁵⁶. In particular, there it is observed that bends occur at resonances $m_{\text{int}} : m_{\text{norm}} : n$ at which the coefficient m_{norm} of the normal frequency fulfills $|m_{\text{norm}}| = 1$. This condition is fulfilled for $\mathcal{M}_1^{\text{fp}}$ crossing the $3 : 1 : 1$ resonance and $\mathcal{M}_2^{\text{fp}}$ crossing the $-1 : 2 : 0$ resonance. A more detailed investigation of the resonance gaps, which also takes into account hyperbolic 1-tori, is left for the future.

III. HIERARCHY OF REGULAR TORI

It is well-established that the phase space of 2D maps generically exhibits a hierarchy^{1,23} of regular tori, i.e., *islands-around-islands* and island chains converging towards an irrational torus. In this case the regular tori are organized around elliptic periodic orbits. We now discuss for 4D maps a hierarchy similar to the islands-around-islands case. Since 2-tori are organized around elliptic 1-tori, it is sufficient to understand the hierarchy of families of elliptic 1-tori. In this sense, these families of elliptic 1-tori correspond to the elliptic periodic orbits in 2D maps.

According to the previous section there are two possible origins for families of elliptic 1-tori: (α) A family emanates from an elliptic-elliptic point or (β) it results from broken resonant 2-tori that fulfilled a rank-1 resonance. The elliptic-elliptic points in case (α) can be either due to ($\alpha 1$) a broken 2-torus that fulfilled a rank-2 resonance, see Appendix B, or ($\alpha 2$) a broken elliptic 1-torus with rational intrinsic frequency $\nu_1 = m/n$, i.e., a rank-1 resonance $m : 0 : n$, see Sec. II E (i).

There is a hierarchical structure, where families of elliptic 1-tori are organized around a family of elliptic 1-tori. Consider such a family of elliptic 1-tori \mathcal{M} with intrinsic frequencies ν_1 , which is surrounded by its two-parameter family of 2-tori \mathcal{T} . The next level of the hierarchy around \mathcal{M} results from three types of structures:

($\alpha 1$) rank-2 resonances in \mathcal{T} , each giving elliptic-elliptic points with two families $\mathcal{M}_1^{\alpha 1}$ and $\mathcal{M}_2^{\alpha 1}$,

($\alpha 2$) rank-1 resonances $m : 0 : n$ on \mathcal{M} , i.e., rational intrinsic frequencies, each giving elliptic-elliptic points with two families $\mathcal{M}_1^{\alpha 2}$ and $\mathcal{M}_2^{\alpha 2}$,

(β) rank-1 resonances in \mathcal{T} , each giving a family \mathcal{M}^β .

Around each of these new families of 1-tori the hierarchy continues with these three types ($\alpha 1$), ($\alpha 2$) and (β) on finer and finer scales. The case ($\alpha 1$) might be seen as a direct generalization of the islands-around-islands hierarchy in 2D maps^{1,23}. It is interesting to observe that in case ($\alpha 2$) the family $\mathcal{M}_1^{\alpha 2}$ is tangential to the family \mathcal{M} ,

looking like an island chain within \mathcal{M} . The other family $\mathcal{M}_2^{\alpha 2}$ coincides with the type (β) family of the rank-1 resonance $m : 0 : n$.

We now explicitly illustrate the hierarchy of 1-tori starting from the elliptic-elliptic fixed point \vec{u}_{fp} with its two Lyapunov families $\mathcal{M}_1^{\text{fp}}$ and $\mathcal{M}_2^{\text{fp}}$ of 1-tori. For all three types of structures Figs. 4 (a), (b), and (c) show 2-tori around \mathcal{M}^7 , \mathcal{M}^{res} , and $\mathcal{M}_{1,2}^{\alpha 2}$ in the 3D phase-space slice and Figs. 4 (d), (e), and (f) show the corresponding frequency planes. For this we calculate the frequencies of each torus with respect to its organizing structure (a similar method has been used for time-continuous systems⁵⁷). That is, for a torus around \mathcal{M}^7 or $\mathcal{M}_{1,2}^{\alpha 2}$ only every 7-th point is used to obtain the frequencies (ν'_1, ν'_2) and (ν''_1, ν''_2) respectively. For a torus around \mathcal{M}^{res} additionally to the frequency $\nu''_1 = \nu_1/3 = \nu_2$ another independent frequency ν''_2 is computed. Fig. 4 provides examples for all three cases:

($\alpha 1$) The families \mathcal{M}_1^7 and \mathcal{M}_2^7 around one of the elliptic-elliptic period-7 orbits lead to \mathcal{C}_1^7 and \mathcal{C}_2^7 in Fig. 4 (a). The regular regions around such an elliptic-elliptic point \vec{u}_{p} and the elliptic-elliptic fixed point \vec{u}_{fp} , see Fig. 1, look qualitatively similar. The same is true for the frequency planes in Figs. 4 (d) and 3.

(β) \mathcal{M}^{res} , which originates from the $-1 : 3 : 0$ resonance, leads to \mathcal{C}^{res} in Fig. 4 (b). The regular regions for such a resonance in Fig. 4 (b) and 4 (e) are different from those shown in Figs. 1, 3, 4 (a), and 4 (d) as there is only one family of 1-tori and only one edge in the frequency plane.

($\alpha 2$) $\mathcal{M}_1^{\alpha 2}$ and $\mathcal{M}_2^{\alpha 2}$ resulted from the intersection of the $7 : 0 : 2$ resonance with $\mathcal{M}_1^{\text{fp}}$ and lead to $\mathcal{C}_1^{\alpha 2}$ and $\mathcal{C}_2^{\alpha 2}$ in Fig. 4 (c). The regular region around $\mathcal{M}_1^{\alpha 2}$ and $\mathcal{M}_2^{\alpha 2}$ in Figs. 4 (c) and (f) looks qualitatively similar to the case ($\alpha 1$). However, one family $\mathcal{M}_1^{\alpha 2}$ leading to the central line $\mathcal{C}_1^{\alpha 2}$ (turquoise) is embedded in a gap of $\mathcal{C}_1^{\text{fp}}$ (orange) in Fig. 4 (c). Consequently, $\mathcal{C}_1^{\alpha 2}$ is quite short. $\mathcal{M}_2^{\alpha 2}$, leading to $\mathcal{C}_2^{\alpha 2}$ (green) in Fig. 4 (c), coincides with the type (β) family originating from the $7 : 0 : 2$ resonance, see Fig. 3. As none of the points of the elliptic-elliptic period-7 orbit lie in the $p_2^* = 0$ slice, see Fig. 2 (a), they are not visible in Fig. 1. Thus, we use in Fig. 4 (c) the slice condition $q_2^* = 0$.

Note that, as in the case of 2D maps, there may be periodic orbits that neither correspond to case ($\alpha 1$) nor ($\alpha 2$). They result from saddle-node bifurcations⁵⁸ and generate their own hierarchy in the above sense. Such bifurcations have to be investigated with parameter studies⁵⁹, which are not performed here.

IV. SUMMARY AND OUTLOOK

In this paper we study the organization of regular tori in a generic 4D map. Using 3D phase-space slices we visualize how the 2-tori are arranged around a skeleton of elliptic 1-tori, which are computed using a new iterative contraction method. This provides a generalization of the

well-known case of 2D maps, where regular tori encircle elliptic fixed points or periodic orbits.

The 1-tori occur in one-parameter families, appearing as Cantor central lines in the 3D phase-space slice. Two types of families can be distinguished: (α) Families emanating from an elliptic-elliptic fixed point or periodic orbit. While this type is known from near-integrable systems to correspond to Lyapunov families of invariant curves, we observe that these families exist far away from the elliptic-elliptic points and continue beyond large resonance gaps. We show that type (β) results from broken resonant 2-tori that fulfilled a rank-1 resonance condition.

The skeleton of 1-tori is interrupted by resonance gaps. We observe two distinct behaviors when a family of 1-tori crosses a resonance: (i) If the resonance involves only the intrinsic frequency of the 1-tori, periodic orbits occur similar to the case of the Poincaré-Birkhoff theorem of 2D maps. (ii) If the resonance involves the normal frequency of the 1-tori, the family may bend on either side of the resonance gap. At low order resonances these bends have substantial impact on the geometry and dynamics in phase space. The two types of families of 1-tori, their interplay with resonances, and the break-up of resonant 2-tori allow for interpreting all observed regular structures. These results also explain the hierarchy of the regular structures and thus generalize the well-known islands-around-islands hierarchy of 2D maps.

As an outlook we mention that it should be possible to extend the results to understand the origin of lower-dimensional tori and their hierarchy in even higher-dimensional systems. Moreover, the visualization of central lines formed by elliptic 1-tori should be complemented by a computation of hyperbolic 1-tori. Another line of investigation is to have a more detailed look at the resonance gaps and bifurcations of the families of 1-tori.

We believe that the computation and visualization of the skeleton of 1-tori can also be useful for other systems like the helium atom, the hydrogen atom in crossed fields, or the restricted three-body problem to understand the organization of regular tori in phase space.

ACKNOWLEDGMENTS

We are grateful for discussions with Jacques Laskar, Jim Meiss, Haris Skokos and Holger Waalkens. We would like to thank the referees for very useful comments. Furthermore, we acknowledge support by the Deutsche Forschungsgemeinschaft within the Forschergruppe 760 ‘‘Scattering Systems with Complex Dynamics.’’ All 3D visualizations were created using MAYAVI⁶⁰.

Appendix A: Computation of elliptic 1-tori

While f -tori in a $2f$ -dimensional phase space can be found by a brute-force search and many algorithms

exist to determine periodic orbits, lower-dimensional tori have to be obtained from more sophisticated algorithms^{27,41,55,61–67}. We present a new approach which is based on an iterative contraction of f -tori to lower-dimensional elliptic tori^{22,68}. One of the advantages of this approach is that it has not to be adjusted for more complicated topologies of 1-tori, i.e., occurring at the resonance gaps, and that it does not require any slices. Moreover, as no continuation is necessary to find families of 1-tori the algorithm is not restricted by large resonance gaps. The basic idea should work for arbitrary dimensions, but for simplicity we only discuss the case $f = 2$.

The idea of the iterative method is to start from a 2-torus and geometrically contract it to a 1-torus, i.e., a 2-torus for which one action is 0: Consider an initial 2-torus T^0 with actions (I_1^0, I_2^0) , corresponding angle coordinates (Θ_1^0, Θ_2^0) , and frequencies (ν_1^0, ν_2^0) . Without loss of generality, we assume that geometrically Θ_1^0 belongs to the major radius of the torus. Starting from an initial point on the torus we obtain an orbit $\vec{x}^0(t)$ and the major frequency ν_1^0 . We determine the times $t_l < t_{\max}$, with $l = 0, 1, \dots, L - 1$, for which the angle coordinates $\Theta_1^0(t)$ of $\vec{x}^0(t)$ are closest to $\Theta_1^0(0)$, i.e.,

$$\Theta_1^0(t_l) - \Theta_1^0(0) = 2\pi\nu_1^0 t_l \bmod 2\pi \approx 0. \quad (\text{A1})$$

The points $\vec{x}^0(t_l)$ differ in their normal angle Θ_2^0 but approximately match in the angle Θ_1^0 . Note that a similar setting is used in time-continuous systems to average out the resonant motion⁵⁷. One could simply use the geometric center of the L points $\vec{x}^0(t_l)$ as a new initial point $\vec{x}^1(0)$ ^{22,68}. Motivated by ellipsoidal approximations⁵⁵, a faster convergence is achieved by fitting 2D ellipses⁶⁹ to the projections of the points $\vec{x}^0(t_l)$ in each degree of freedom. Their centers define the new initial point $\vec{x}^1(0)$. The orbit $\vec{x}^1(t)$ for this point lies supposedly on a similar 2-torus T^1 with smaller action $I_2^1 < I_2^0$. Iterating these steps N times gives a sequence of 2-tori T^i approaching a 1-torus. By construction the frequency ν_1^i and action I_1^i of the 2-tori T^i converge to those of the 1-torus.

A problem common to all methods computing lower-dimensional tori is to decide whether the result is close enough to a 1-torus, ideally by estimating the minor radius. For this, we try to approximate the orbit $\vec{x}^N(t)$ on the final torus T^N by a Fourier series^{62,64,70}

$$\vec{x}(t) = \sum_{|k| \leq k_{\max}} \vec{c}_k e^{i2\pi k \nu_1^N t}, \quad (\text{A2})$$

for $t < \tau$. If the maximal square deviation $\sigma_\tau^2 = \sup_{t < \tau} \|\vec{x}(t) - \vec{x}^N(t)\|^2$ of the Fourier series is smaller than a prescribed value σ_{\max}^2 , the torus T^N is considered to be a 1-torus. However, even if this criterion is fulfilled for a chosen τ the actual torus may still have a large minor radius. This becomes only apparent when using more iterations $t > \tau$. Such a torus usually has frequencies close to a rank-1 resonance. Thus, additionally we use the maximal square deviation $\sigma_{4\tau}^2 = \sup_{t < 4\tau} \|\vec{x}(t) - \vec{x}^N(t)\|^2$

with the previous Fourier series $\vec{x}(t)$ obtained from $t < \tau$. A torus is discarded if the ratio $R_{\sigma^2} = \sigma_{4\tau}^2 / \sigma_\tau^2$ is bigger than R_{\max} . In such cases one could also increase t_{\max} to obtain a better converged torus.

To obtain the 1-tori used in this paper we start from approximately $3 \cdot 10^6$ 2-tori, see Sec. II C, and for each of them use initially $N = 10$, $L = 10$, $t_{\max} = 2^{14}$, $\tau = 4096$, and the smallest $k_{\max} \in [40, 80, 160, 320, 400]$ for which $\sigma_\tau^2 < \sigma_{\max}^2 = 10^{-10}$ and $R_{\sigma^2} < R_{\max} = 2.25$ is fulfilled. If these criteria fail the computation is repeated one more time with doubled t_{\max} . Since the algorithm sometimes converges to periodic orbits, also 1-tori with near-rational major frequency ν_1^N are excluded. That is, if the highest convergent a/b , $a, b \in \mathbb{N}$ of a continued fraction expansion of ν_1^N with $b < 500$ (or $b < 3500$ for the period-7 island) fulfills $|\nu_1^N - a/b| < 10^{-10}$ it is discarded. Finally, the intersections of converged tori with the 3D phase-space slice are obtained by linear interpolation using 10^4 iterates of each torus. The result is accepted if the points used for the interpolation are closer to the slice than 10^{-3} . Larger distances result from a near-rational major frequency and could be treated by using more iterates or higher order interpolation methods. Some converged tori intersect the slice more often due to strong bends or a shallow intersection angle. To display only the main skeleton of 1-tori, we excluded such tori if in case of $\mathcal{M}_1^{\text{fp}}$ and $\mathcal{M}_2^{\text{fp}}$, any of their intersections with the slice does not fulfill $|p_1| < 10^{-3}$ and, in case of \mathcal{M}^{res} , none of the intersections fulfills $|p_1| < 10^{-3}$.

An advantage of the algorithm is that only the major frequency ν_1 has to be computed correctly to obtain the right central lines: For example to get the Lyapunov families of the elliptic-elliptic fixed point \vec{u}_{fp} the frequency with largest amplitude is used. For the Lyapunov families of the elliptic-elliptic period-7 orbits the frequency with largest amplitude with respect to the 7-th iterate of the map is chosen. For the $-1 : 3 : 0$ resonance the frequency $\nu_1/3 = \nu_2$ is used. Note that the algorithm can also converge to 1-tori of rank-1 resonances $m_1 : m_2 : n$ at which the coefficient m_2 of the normal frequency, or in this context minor frequency, fulfills $|m_2| = 1$, e.g., the $7 : 1 : 2$ resonance at $\mathcal{M}_1^{\text{fp}}$. These 1-tori have been omitted in the figures for simplicity.

Appendix B: Break-up of resonant 2-tori

In this section, we briefly review and illustrate the results of Todesco about the break-up of resonant 2-tori of an integrable 4D symplectic map when a perturbation is added³⁰. These results are derived for the vicinity of an elliptic-elliptic fixed point, but we find the described behavior for resonant tori far away from a fixed point or even in the absence of a fixed point. Also, the examples demonstrate how the geometry of the original resonant 2-torus governs the geometry of the phase-space structures remaining after the break-up. Additionally, the break-up of a 1-torus with rational intrinsic frequency is presented,

a case not discussed by Todesco.

The break-up of a resonant 2-torus in a 4D symplectic map depends on the number k of fulfilled, linearly independent resonance conditions, Eq. (4), denoted as *rank* k , and whether the resonance is *coupled* or *uncoupled*. The four possible cases are illustrated by examples in phase space and the frequency plane, see Fig. 5. The example tori are chosen as close as possible to each other such that the geometry of the unbroken tori resemble each other. Thus, they look like different cases of resonances for geometrically the same torus.

a. Rank-0: On a non-resonant 2-torus of the integrable system each orbit is dense. Such a 2-torus will in general survive a perturbation and just be deformed (KAM-theorem). An example is shown in Fig. 5 (b) and marked as point (b) in Fig. 5 (a). Such 2-tori have been called *rotational*^{46,71}.

b. Rank-1, uncoupled: If one uncoupled resonance condition $m_1\nu_1 = n$ with $m_1 \neq 0$ is fulfilled on a 2-torus of the integrable system, each orbit on it densely fills m_1 disjunct lines. At least $2m_1$ of these infinite number of lines survive a perturbation, alternating between normally elliptic and normally hyperbolic⁷². An example is shown in Fig. 5 (c) and marked as point (c) in Fig. 5 (a). The original 2-torus broke since it was on the $7 : 0 : 2$ resonance leaving a 1-torus consisting of seven elliptic lines (hyperbolic lines not shown). This 1-torus is displayed in Fig. 5 (c) along with a 2-torus from its elliptic surrounding. In this example there are another seven elliptic lines (not shown).

c. Rank-1, coupled: If one coupled resonance condition Eq. (4) with both m_1 and m_2 nonzero is fulfilled on a 2-torus of the integrable system, each orbit on it densely fills a line. At least one elliptic and one hyperbolic line survive a perturbation. An example is shown in Fig. 5 (d) and marked as point (d) in Fig. 5 (a). The original 2-torus broke since it was on the $-1 : 3 : 0$ resonance leaving one elliptic line (hyperbolic line not shown). This 1-torus and a thin 2-torus from its elliptic surrounding are displayed in Fig. 5 (d). Such 2-tori of rank-1 resonances have been called *tube tori*^{46,71}.

d. Rank-2: If two independent resonance conditions Eq. (4) are fulfilled on a 2-torus of the integrable system, each orbit on it is periodic. If the resonance is at $(\nu_1 = \frac{n_1}{m_1}, \nu_2 = \frac{n_2}{m_2})$ then the period is given by $\text{lcm}(m_1, m_2)$. At least four periodic orbits survive a perturbation: either one elliptic-elliptic, one hyperbolic-hyperbolic, and two elliptic-hyperbolic periodic orbits or two complex unstable and two elliptic-hyperbolic periodic orbits. Such a break-up has also been derived from symmetry considerations⁵⁸ and has been analyzed also for the case of strong resonances⁷³. An example for a rank-2 resonance is shown in Fig. 5 (e) and marked as point (e) in Fig. 5 (a). The original 2-torus broke since it was at the intersection of the resonances $7 : 0 : 2$ and $-1 : 3 : 0$ leaving two elliptic-elliptic, two hyperbolic-hyperbolic, and four elliptic-hyperbolic periodic orbits of period 21. The twofold number of periodic orbits is

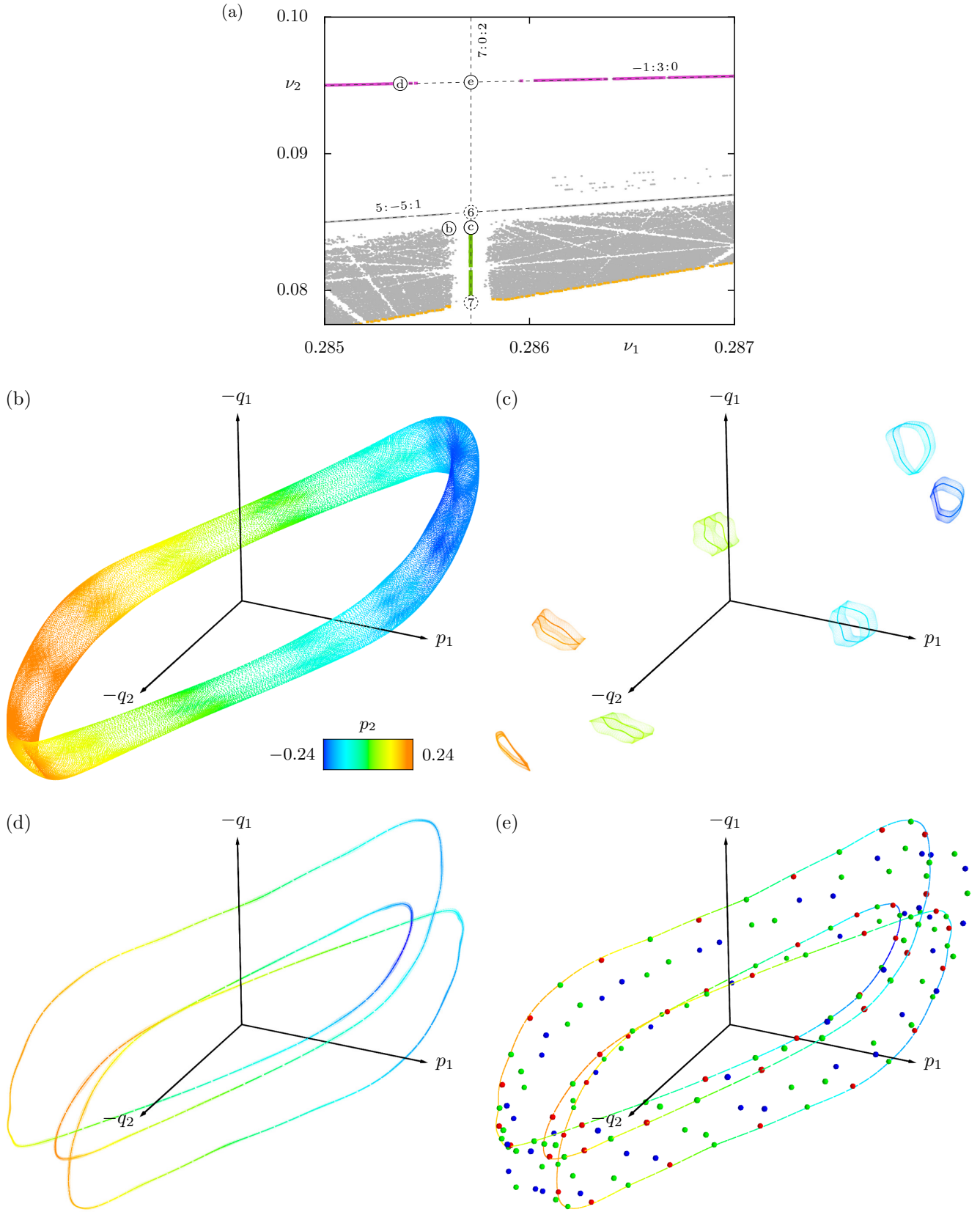


FIG. 5. Illustration of the break-up of resonant 2-tori. (a) Magnification of the frequency plane shown in Fig. 3. The circled small letters mark the frequencies of the example tori for the different cases (b)–(e) and Figs. 6 and 7. The example tori are visualized by 3D projections as in Fig. 2: (b) irrational torus, (c) elliptic 1-torus of the uncoupled rank-1 resonance $7 : 0 : 2$ with a 2-torus from its surrounding, (d) elliptic 1-torus of the coupled rank-1 resonance $-1 : 3 : 0$ with a thin 2-torus from its surrounding, (e) two elliptic-elliptic (red), four elliptic-hyperbolic (green) and two hyperbolic-hyperbolic (blue) periodic orbits of period 21 from the rank-2 resonance at $(\nu_1, \nu_2) = (2/7, 2/21)$. The 1-torus of (d) is shown for comparison. For a rotating view see⁷⁴

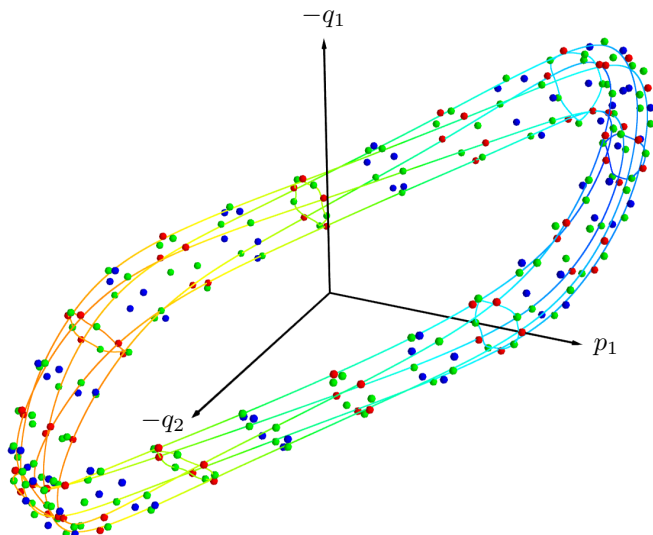


FIG. 6. Rank-2 resonance $(\nu_1, \nu_2) = (2/7, 3/35)$ at the intersection of the resonances $5 : -5 : 1$ and $7 : 0 : 2$ marked as point (6) in Fig. 5 (a). Shown are two elliptic-elliptic (red), four elliptic-hyperbolic (green) and two hyperbolic-hyperbolic (blue) periodic orbits of period 35. A 1-torus of the $5 : -5 : 1$ resonance and the 1-torus of Fig. 5 (c) are shown for comparison. For a rotating view see⁷⁴

analogous to the twofold number of surviving 1-tori for the $7 : 0 : 2$ resonance. Another example for a rank-2 resonance are the period-7 orbits the central lines \mathcal{C}^7 in Fig. 1 originate from. These periodic orbits result from the rank-2 resonance at the intersection of the resonances $7 : 0 : 2$ and $3 : 1 : 1$, see Fig. 3.

For reasons of continuity we expect the periodic orbits of a rank-2 resonance to be located where the surviving lines of the two crossing rank-1 resonances get close to each other in phase space. For example, we expect an elliptic-elliptic periodic orbit, where an elliptic line of the first rank-1 resonance and an elliptic line of the second one get close to each other. This is nicely illustrated by the rank-2 resonance in Fig. 6. There each of the elliptic 1-tori of the $5 : -5 : 1$ and $7 : 0 : 2$ resonances almost coincides with a chain of alternating elliptic-elliptic and elliptic-hyperbolic periodic orbits. Elliptic-elliptic points occur where these elliptic 1-tori almost intersect. Note again that there exists another elliptic 1-torus from the $7 : 0 : 2$ resonance in between the shown ones.

From this argument also the number and stability of periodic orbits resulting from a rank-2 resonance becomes plausible: The elliptic (E_1) and the hyperbolic (H_1) line of the first rank-1 resonance intersect in four kind of points with the elliptic (E_2) and hyperbolic (H_2) line of the second rank-1 resonance, giving periodic orbits with stability E_1E_2 , E_1H_2 , E_2H_1 , and H_1H_2 .

As discussed in Secs. II E (i) and III a one dimensional chain of elliptic-elliptic and elliptic-hyperbolic periodic orbits arises from the break-up of an elliptic 1-torus with rational intrinsic frequency. This case is illustrated in

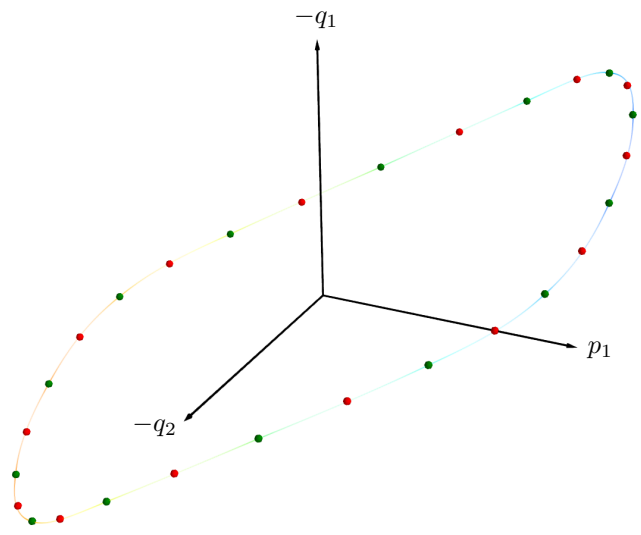


FIG. 7. One-dimensional chain of periodic orbits at the intersection of the rank-1 resonance $7 : 0 : 2$ and the family of elliptic 1-tori $\mathcal{M}_1^{\text{fp}}$ marked as point (7) in Fig. 5 (a). Shown are two elliptic-elliptic (red) and two elliptic-hyperbolic (green) periodic orbits of period 7 (also shown in Fig. 2 (a)). A 1-torus of $\mathcal{M}_1^{\text{fp}}$ close to the intersection is shown for comparison. For a rotating view see⁷⁴

Fig. 7 for the intersection of the $7 : 0 : 2$ resonance and $\mathcal{M}_1^{\text{fp}}$.

- ¹A. J. Lichtenberg and M. A. Leibermann, *Regular and chaotic dynamics*, Springer-Verlag, New York, second ed. (1992)
- ²S. Udry and D. Pfenniger, “Stochasticity in elliptical galaxies”, *Astron. & Astrophys.* **198**, 135–149 (1988)
- ³J. Laskar, “The chaotic motion of the solar system: A numerical estimate of the size of the chaotic zones”, *Icarus* **88**, 266–291 (1990)
- ⁴P. M. Cincotta, “Arnold diffusion: an overview through dynamical astronomy”, *New Astron. Rev.* **46**, 13–39 (2002)
- ⁵H. S. Dumas and J. Laskar, “Global dynamics and long-time stability in Hamiltonian systems via numerical frequency analysis”, *Phys. Rev. Lett.* **70**, 2975–2979 (1993)
- ⁶K. Richter and D. Wintgen, “Stable planetary atom configurations”, *Phys. Rev. Lett.* **65**, 1965 (1990)
- ⁷P. Schlagheck and A. Buchleitner, “Stable classical configurations in strongly driven helium”, *Physica D* **131**, 110–124 (1999)
- ⁸S. Gekle, J. Main, T. Bartsch, and T. Uzer, “Extracting multidimensional phase space topology from periodic orbits”, *Phys. Rev. Lett.* **97**, 104101 (2006)
- ⁹S. Keshavamurthy, “Dynamical tunneling in molecules: quantum routes to energy flow”, *Int. Rev. Phys. Chem.* **26**, 521–584 (2007)
- ¹⁰R. Paškauskas, C. Chandre, and T. Uzer, “Dynamical bottlenecks to intramolecular energy flow”, *Phys. Rev. Lett.* **100**, 083001 (2008)
- ¹¹H. Waalkens, R. Schubert, and S. Wiggins, “Wigner’s dynamical transition state theory in phase space: classical and quantum”, *Nonlinearity* **21**, R1–R118 (2008)
- ¹²S. M. Graff, “On the conservation of hyperbolic invariant tori for Hamiltonian systems”, *J. Diff. Eqs.* **15**, 1–69 (1974)
- ¹³E. Zehnder, “Generalized implicit function theorems with applications to some small divisor problems, II”, *Comm. Pure Appl. Math.* **29**, 49–111 (1976)
- ¹⁴J. Pöschel, “On elliptic lower dimensional tori in Hamiltonian systems”, *Math. Z.* **202**, 559–608 (1989)

- ¹⁵À. Jorba and J. Villanueva, “On the persistence of lower dimensional invariant tori under quasi-periodic perturbations”, *J. Nonlinear Sci.* **7**, 427–473 (1997)
- ¹⁶V. I. Arnold, “Instability of dynamical systems with several degrees of freedom”, *Sov. Math. Dokl.* **5**, 581–585 (1964)
- ¹⁷B. V. Chirikov, “A universal instability of many-dimensional oscillator systems”, *Phys. Rep.* **52**, 263–379 (1979)
- ¹⁸M. Ding, T. Bountis, and E. Ott, “Algebraic escape in higher dimensional Hamiltonian systems”, *Phys. Lett. A* **151**, 395–400 (1990)
- ¹⁹E. G. Altmann, A. E. Motter, and H. Kantz, “Stickiness in Hamiltonian systems: From sharply divided to hierarchical phase space”, *Phys. Rev. E* **73**, 026207 (2006)
- ²⁰E. G. Altmann and H. Kantz, “Hypothesis of strong chaos and anomalous diffusion in coupled symplectic maps”, *Europhys. Lett.* **78**, 10008 (2007)
- ²¹D. L. Shepelyansky, “Poincaré recurrences in Hamiltonian systems with a few degrees of freedom”, *Phys. Rev. E* **82**, 055202 (2010)
- ²²S. Lange, Diploma thesis, Technische Universität Dresden, Fachrichtung Physik (2012)
- ²³J. D. Meiss, “Class renormalization: Islands around islands”, *Phys. Rev. A* **34**, 2375–2383 (1986)
- ²⁴L. H. Eliasson, “Perturbations of stable invariant tori for Hamiltonian systems”, *Ann. Sc. Norm. Super. Pisa, Cl. Sci.* **15**, 115–147 (1988)
- ²⁵M. B. Sevryuk, “Invariant tori of intermediate dimensions in Hamiltonian systems”, *Regular and Chaotic Dynamics* **2**, 30–40 (1997)
- ²⁶À. Jorba and J. Villanueva, “On the normal behaviour of partially elliptic lower-dimensional tori of Hamiltonian systems”, *Nonlinearity* **10**, 783–822 (1997)
- ²⁷À. Jorba and M. Ollé, “Invariant curves near Hamiltonian-Hopf bifurcations of four-dimensional symplectic maps”, *Nonlinearity* **17**, 691–710 (2004)
- ²⁸M. Sevryuk, “KAM tori: persistence and smoothness”, *Nonlinearity* **21**, T177–T185 (2008)
- ²⁹À. Jorba and J. Villanueva, “The fine geometry of the Cantor families of invariant tori in Hamiltonian systems”, in “European Congress of Mathematics”, edited by C. Casacuberta, R. Miró-Roig, J. Verdera, and S. Xambó-Descamps, Birkhäuser Basel, vol. 202 of *Progress in Mathematics*, pp. 557–564 (2001)
- ³⁰E. Todesco, “Analysis of resonant structures of four-dimensional symplectic mappings, using normal forms”, *Phys. Rev. E* **50**, R4298–R4301 (1994)
- ³¹A. Luque and J. Villanueva, “A KAM theorem without action-angle variables for elliptic lower dimensional tori”, *Nonlinearity* **24**, 1033–1080 (2011)
- ³²D. Pfenniger, “Numerical study of complex instability. I. Mappings”, *Astron. & Astrophys.* **150**, 97–111 (1985)
- ³³T. K. Roy and A. Lahiri, “Reversible Hopf bifurcation in four-dimensional maps”, *Phys. Rev. A* **44**, 4937–4944 (1991)
- ³⁴A. Lahiri, A. Bhowal, and T. K. Roy, “Resonant collisions in four-dimensional reversible maps: A description of scenarios”, *Physica D* **112**, 95–116 (1998)
- ³⁵A. Morbidelli and A. Giorgilli, “Superexponential stability of KAM tori”, *J. Stat. Phys.* **78**, 1607–1617 (1995)
- ³⁶E. G. Altmann, A. E. Motter, and H. Kantz, “Stickiness in mushroom billiards”, *Chaos* **15**, 033105 (2005)
- ³⁷L. Bunimovich, “Relative volume of Kolmogorov-Arnold-Moser tori and uniform distribution, stickiness and nonstickiness in Hamiltonian systems”, *Nonlinearity* **21**, T13–T17 (2008)
- ³⁸S. Gekle, J. Main, T. Bartsch, and T. Uzer, “Hydrogen atom in crossed electric and magnetic fields: Phase space topology and torus quantization via periodic orbits”, *Phys. Rev. A* **75**, 023406 (2007)
- ³⁹M. Sevryuk and A. Lahiri, “Bifurcations of families of invariant curves in four-dimensional reversible mappings”, *Phys. Lett. A* **154**, 104–110 (1991)
- ⁴⁰M. N. Vrahatis, H. Isliker, and T. C. Bountis, “Structure and breakdown of invariant tori in a 4-D mapping model of accelerator dynamics”, *Int. J. Bifurcat. Chaos* **07**, 2707–2722 (1997)
- ⁴¹J. Couetdic, J. Laskar, A. C. M. Correia, M. Mayor, and S. Udry, “Dynamical stability analysis of the HD 202206 system and constraints to the planetary orbits”, *Astron. & Astrophys.* **519**, A10 (2010)
- ⁴²M. Richter, S. Lange, A. Bäcker, and R. Ketzmerick, “Visualization and comparison of classical structures and quantum states of four-dimensional maps”, *Phys. Rev. E* **89**, 022902 (2014)
- ⁴³J. Laskar, “Frequency analysis for multi-dimensional systems: global dynamics and diffusion”, *Physica D* **67**, 257–281 (1993)
- ⁴⁴C. Froeschlé, “Numerical study of a four-dimensional mapping”, *Astron. & Astrophys.* **16**, 172–189 (1972)
- ⁴⁵P. A. Patsis and L. Zachilas, “Using color and rotation for visualizing four-dimensional Poincaré cross-sections: With applications to the orbital behavior of a three-dimensional Hamiltonian system”, *Int. J. Bifurcat. Chaos* **4**, 1399–1424 (1994)
- ⁴⁶M. Katsanikas and P. A. Patsis, “The structure of invariant tori in a 3D galactic potential”, *Int. J. Bifurcat. Chaos* **21**, 467–496 (2011)
- ⁴⁷Note that intersections of two objects in a 3D projection are only real intersections in the full 4D phase space, if the colors match at an intersection point.
- ⁴⁸K. Meyer, G. Hall, and D. Offin, *Introduction to Hamiltonian Dynamical Systems and the N-Body Problem*, Springer-Verlag, New York (2009)
- ⁴⁹M. Sevryuk, “On invariant tori of reversible systems in the neighbourhood of an equilibrium position”, *Russ. Math. Surv.* **42**, 147–148 (1987)
- ⁵⁰M. Sevryuk, “Invariant m-dimensional tori of reversible systems with phase space of dimension greater than 2m”, *J. Sov. Math.* **51**, 2374–2386 (1990)
- ⁵¹R. Bartolini, A. Bazzani, M. Giovannozzi, W. Scandale, and E. Todesco, “Tune evaluation in simulations and experiments”, *Part. Accel.* **52**, 147–177 (1996)
- ⁵²M. Born, *The Mechanics of the Atom*, G. Bell And Sons, LTD, London (1927)
- ⁵³H. R. Dullin and J. D. Meiss, “Twist singularities for symplectic maps”, *Chaos* **13**, 1–16 (2003)
- ⁵⁴À. Jorba, “Numerical computation of the normal behaviour of invariant curves of n-dimensional maps”, *Nonlinearity* **14**, 943–976 (2001)
- ⁵⁵H. R. Dullin and J. D. Meiss, “Quadratic volume-preserving maps: Invariant circles and bifurcations”, *SIAM J. on Applied Dynamical Systems* **8**, 76–128 (2009)
- ⁵⁶H. Broer, H. Hanßmann, À. Jorba, J. Villanueva, and F. Wagener, “Normal-internal resonances in quasi-periodically forced oscillators: a conservative approach”, *Nonlinearity* **16**, 1751–1791 (2003)
- ⁵⁷Y. Papaphilippou and J. Laskar, “Global dynamics of triaxial galactic models through frequency map analysis”, *Astron. & Astrophys.* **329**, 451–481 (1998)
- ⁵⁸H.-t. Kook and J. D. Meiss, “Periodic orbits for reversible, symplectic mappings”, *Physica D* **35**, 65–86 (1989)
- ⁵⁹J.-M. Mao, I. I. Satija, and B. Hu, “Evidence for a new period-doubling sequence in four-dimensional symplectic maps”, *Phys. Rev. A* **32**, 1927–1929 (1985)
- ⁶⁰P. Ramachandran and G. Varoquaux, “Mayavi: 3D visualization of scientific data”, *Comput. Sci. Eng.* **13**, 40–51 (2011)
- ⁶¹C. Simó, “Effective computations in celestial mechanics and astrodynamics”, in “Modern Methods of Analytical Mechanics and their Applications”, edited by V. V. Rumyantsev and A. V. Karapetyan, Springer Verlag, Wien, vol. 387 of *CISM Courses and Lectures*, pp. 55–102 (1998)
- ⁶²E. Castellà and À. Jorba, “On the vertical families of two-dimensional tori near the triangular points of the bicircular problem”, *Celest. Mech. Dyn. Astr.* **76**, 35–54 (2000)
- ⁶³F. Schilder, H. M. Osinga, and W. Vogt, “Continuation of quasi-periodic invariant tori”, *SIAM J. on Applied Dynamical Systems* **4**, 459–488 (2005)

- ⁶⁴Y. Lan, C. Chandre, and P. Cvitanović, “Newton’s descent method for the determination of invariant tori”, *Phys. Rev. E* **74**, 046206 (2006)
- ⁶⁵A. Haro and R. de la Llave, “A parameterization method for the computation of invariant tori and their whiskers in Quasi-Periodic maps: Explorations and mechanisms for the breakdown of hyperbolicity”, *SIAM J. on Applied Dynamical Systems* **6**, 142–207 (2007)
- ⁶⁶M. Sansottera, U. Locatelli, and A. Giorgilli, “A semi-analytic algorithm for constructing lower dimensional elliptic tori in planetary systems”, *Celest. Mech. Dyn. Astr.* **111**, 337–361 (2011)
- ⁶⁷G. Huguet, R. de la Llave, and Y. Sire, “Computation of whiskered invariant tori and their associated manifolds: New fast algorithms”, *Discrete and Continuous Dynamical Systems* **32**, 1309–1353 (2012)
- ⁶⁸F. Onken, Bachelor thesis, Technische Universität Dresden, Fachrichtung Physik (2012)
- ⁶⁹A. W. Fitzgibbon, M. Pilu, and R. B. Fisher, “Direct least-squares fitting of ellipses”, *IEEE Transactions on Pattern Analysis and Machine Intelligence* **21**, 476–480 (1999)
- ⁷⁰A. Bazzani, L. Bongini, and G. Turchetti, “Analysis of resonances in action space for symplectic maps”, *Phys. Rev. E* **57**, 1178–1180 (1998)
- ⁷¹M. N. Vrahatis, T. C. Bountis, and M. Kollmann, “Periodic orbits and invariant surfaces of 4d nonlinear mappings”, *Int. J. Bifurcat. Chaos* **6**, 1425–1437 (1996)
- ⁷²E. Todesco, “Local analysis of formal stability and existence of fixed points in 4d symplectic mappings”, *Physica D* **95**, 1–12 (1996)
- ⁷³V. Gelfreich, C. Simó, and A. Vieiro, “Dynamics of symplectic maps near a double resonance”, *Physica D* **243**, 92–110 (2013)
- ⁷⁴For a rotating view see <http://www.comp-phys.tu-dresden.de/supp/>